Supporting Information

Studies on Chemical Reactivity and Electrocatalysis of Two Acylmethyl(hydroxymethyl)pyridine Ligand-Containing [Fe]-Hydrogenase Models (2-$COCH_2$-6-$HOCH_2C_5H_3N$)$Fe(CO)_2$L (L = η^1-SCOMe, η^1-2-SC_5H_4N)

Li-Cheng Song,*[†,‡] Liang Zhu,[†] Fu-Qiang Hu,[†] and Yong-Xiang Wang[†]

[†]Department of Chemistry, State Key Laboratory of Elemento-Organic Chemistry, College of Chemistry and [‡]Collaborative Innovation Center of Chemical Science and Engineering (Tianjin), Nankai University, Tianjin 300071, China

Contents:

1. Figure S1: Molecular structure of **A**

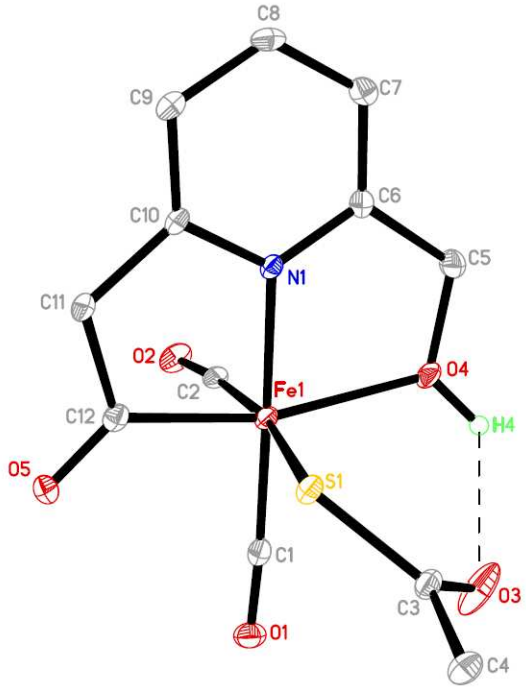

Figure S1. Molecular structure of **A** with ellipsoids drawn at a 30% probability level. All hydrogen atoms are omitted for clarity except the hydroxy H4 atom. Selected bond lengths [Å] and bond angles [°]:Fe(1)–C(12) 1.924(3), Fe(1)–N(1) 1.947(3), Fe(1)–O(4) 2.128(3); C(12)–Fe(1)–S(1) 84.02(11), N(1)–Fe(1)–O(4) 78.13(11).

2. Figure S2: Bulk electrolysis for the two-electron reduction of $[CpFe(CO)_2]_2$ and the one-electron reductions of **A** and **B.**

The reduction event for **A** or **B** is a one-electron process since the final Q values for **A** and **B** determined by bulk electrolysis are both close to half that of the known two-electron reduction of dimer $[CpFe(CO)_2]_2$.[1,2]

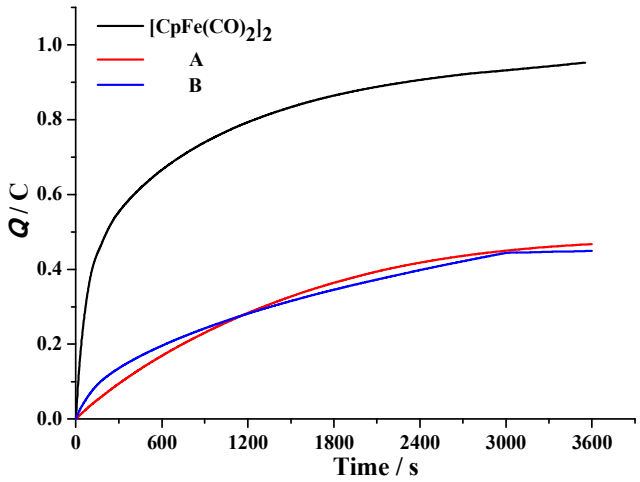

Figure S2. Bulk electrolysis for the two-electron reduction of $[CpFe(CO)_2]_2$ and the one-electron reductions of **A** and **B**.

3. Figure S3: Bulk electrolysis for the two-electron reduction of $[CpFe(CO)_2]_2$ and the one-electron oxidations of **A** and **B.**

The oxidation event for **A** or **B** is a one-electron process since the final Q values for **A** and **B** determined by bulk electrolysis are both close to half that of the known two-electron reduction of dimer $[CpFe(CO)_2]_2$.[1,2]

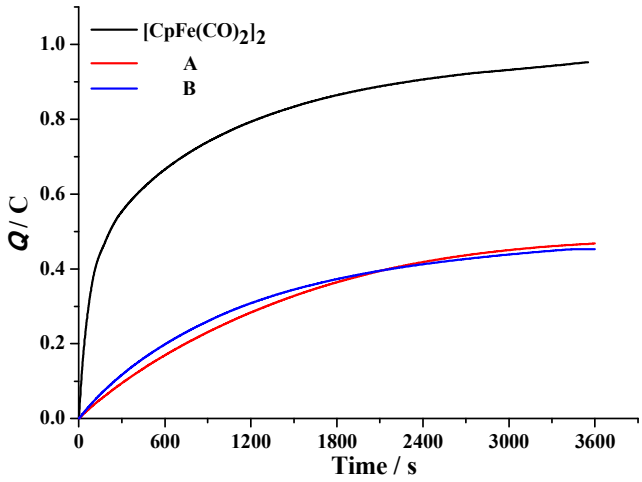

Figure S3. Bulk electrolysis for the two-electron reduction of $[CpFe(CO)_2]_2$ and the one-electron oxidations of **A** and **B**.

4. Figure S4: Plots of i_p versus $\nu^{1/2}$ for the reduction peaks of **A** and **B.**

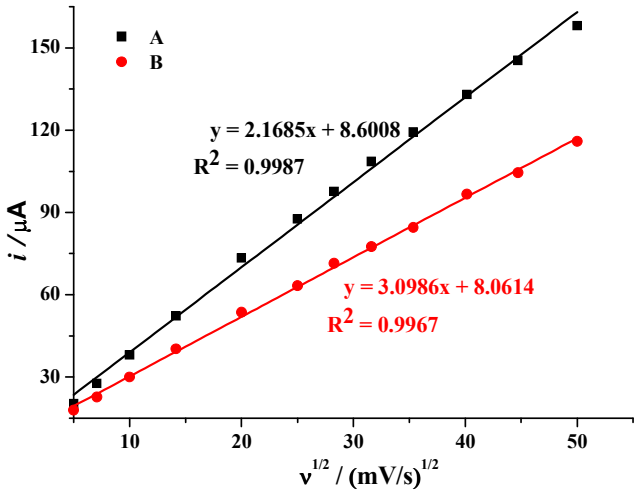

Figure S4. Plots of i_p versus $\nu^{1/2}$ for the reduction peaks of **A** (▪) and **B** (●).

5. **Figure S5:** Cyclic voltammograms of 20 mM TFA in the presence of catalyst **B** and without **B** for calculation of turnover frequency.

Turnover frequency (TOF) was calculated using eq. S1 and was corrected for background acid.[3-5] The normally used i_{cat}/i_p was corrected as shown in eq. S1 and Figure S4 since the overlap of the current density of the acid without any catalyst with the current density of the acid with the catalyst. In equation S1, ν is the scan rate in V/s, i_{cat} is the measured current with added acid in µA, i_{acid} is the measured current of acid by itself at the potential of i_{cat} in µA, i_p is the measured current of catalyst without acid in µA.

$$TOF = 1.94V^{-1} \times \nu \times [(i_{cat}-i_{acid})/i_p]^2 \qquad \text{eq. S1}$$

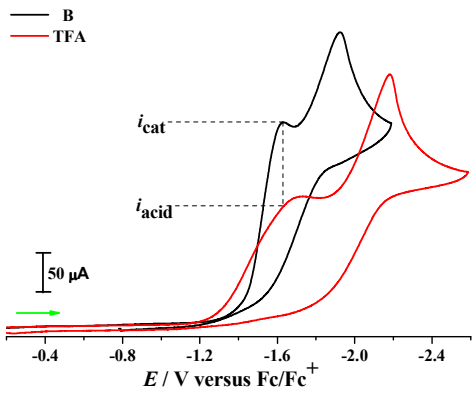

Figure S5. Cyclic voltammograms of **B** (1.0 mM) with 20 mM TFA in 0.1 M *n*-Bu_4NPF_6/MeCN at a scan rate of 0.1 Vs^{-1} (black trace) and 20 mM TFA without the catalyst (red trace).

6. Figures S6 and S7: Overpotential determinations for **A** and **B.**

The overpotentials of **A** and **B** were calculated according to eqs. S2 and S3, where $E_{1/2}{}^{T}$ is equal to the thermodynamic potential for hydrogen production from TFA with the effects of homoconjugation taken into account (for 0.3 M TFA in MeCN referenced to Fc/Fc^{+}, this value is -0.64 V), and $E_{cat/2}$ is the potential at half-maximum of the catalytic current of complex **A** or **B** with TFA.[6-8] The overpotentials for both complexes were measured in the presence of 0.3 M TFA. In equation S2, $E^{0}{}_{H^{+}/H2}$ is the standard potential for the reduction of protons in V, R is the ideal gas constant in $K^{-1}mol^{-1}$, T is the absolute temperature in K, F is Faraday's constant in C/mol, ε_D is a measure of how fast is the diffusion of the products with respect to that of the reactant in V, K_C is association constant, C_0 is the total concentration of the acid in mol/L, $C^{0}{}_{H2}$ is the concentration of dissolved hydrogen corresponding to a partial pressure of 10^5 Pa in mol/L.

$$E_{1/2}{}^{T} = E^{0}{}_{H^{+}/H2} - (2.303RT/F)\,pK_a + \varepsilon_D + (RT/2F)\ln(2K_C{}^{2}C_0C^{0}{}_{H2}) \qquad \text{eq. S2}$$

$$\text{overpotential} = |\,E_{1/2}{}^{T} - E_{cat/2}\,| \qquad \text{eq. S3}$$

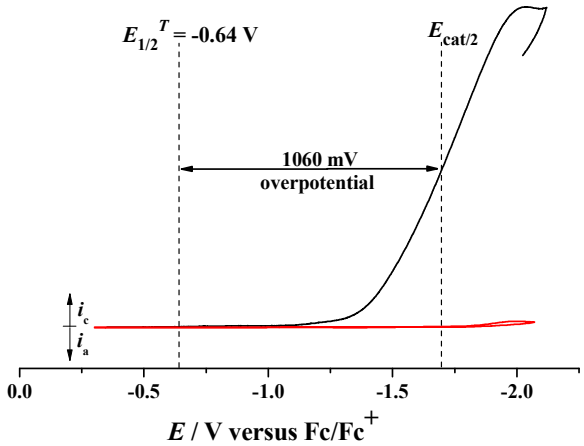

Figure S6. Cyclic voltammograms of **A** (1.0 mM) with TFA (0, 0.3 M) in 0.1 M n-Bu_4NPF_6/MeCN at a scan rate of 0.1 Vs^{-1}.

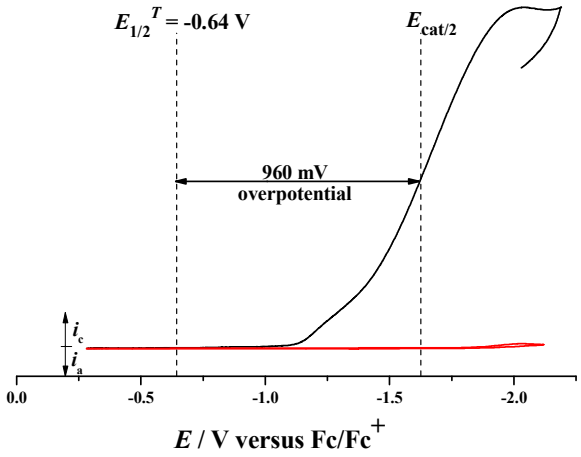

Figure S7. Cyclic voltammograms of **B** (1.0 mM) with TFA (0, 0.3 M) in 0.1 M *n*-Bu_4NPF_6/MeCN at a scan rate of 0.1 Vs^{-1}.

7. Figures S8–S10 IR and ^{1}H (^{13}C) NMR spectra of **B**

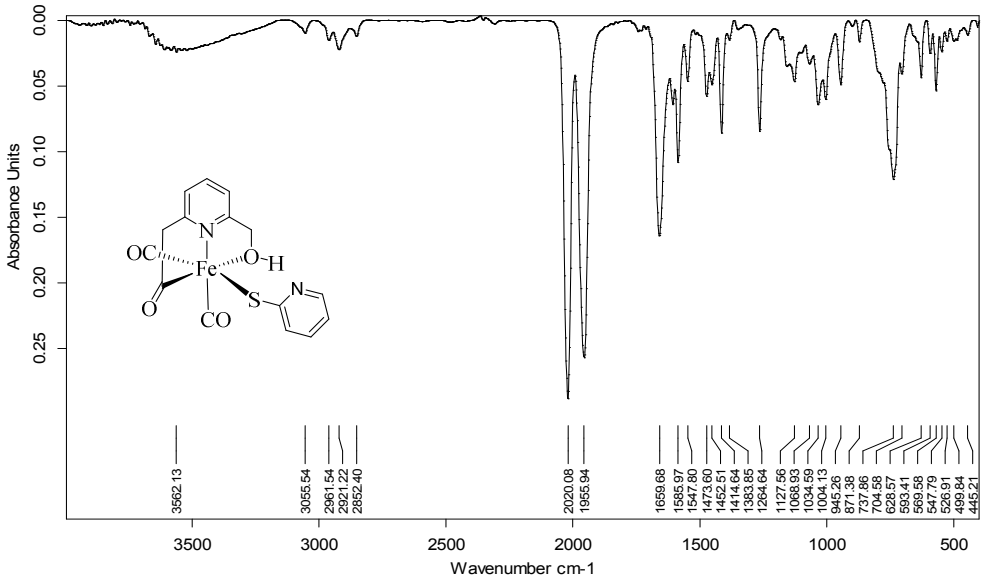

Figure S8. IR spectrum of **B**

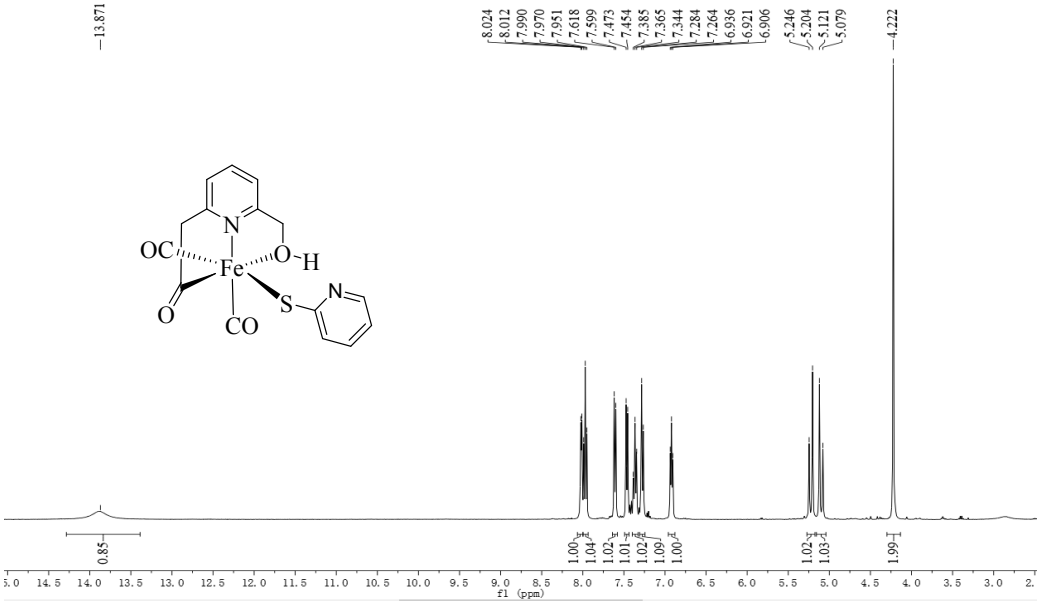

Figure S9. ^{1}H NMR spectrum of **B**

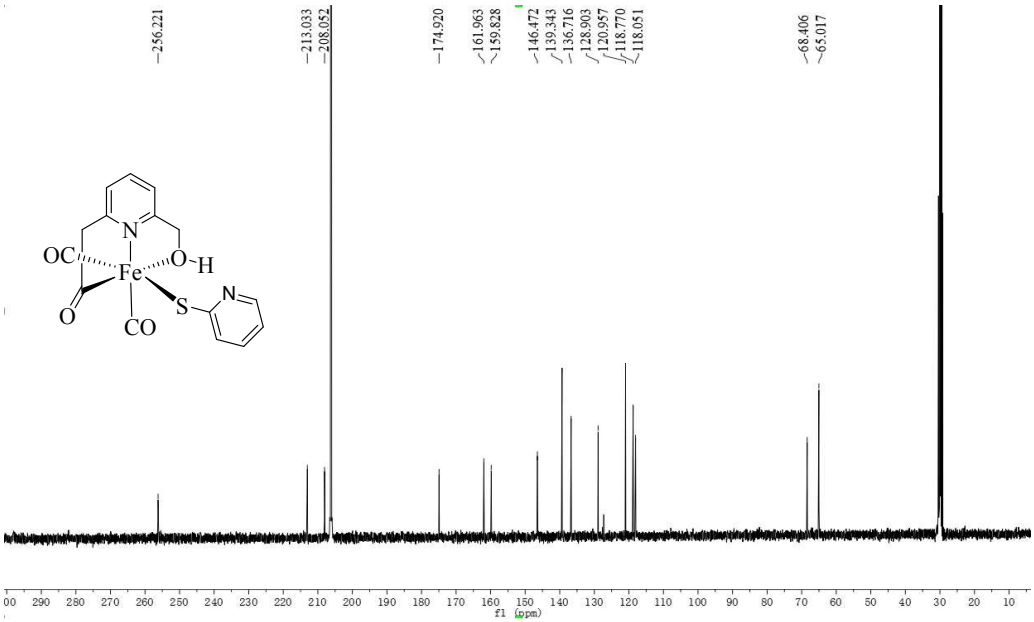

Figure S10. ^{13}C NMR spectrum of **B**

8. Figures S11–S13 IR and ^{1}H (^{13}C) NMR spectra of **1**

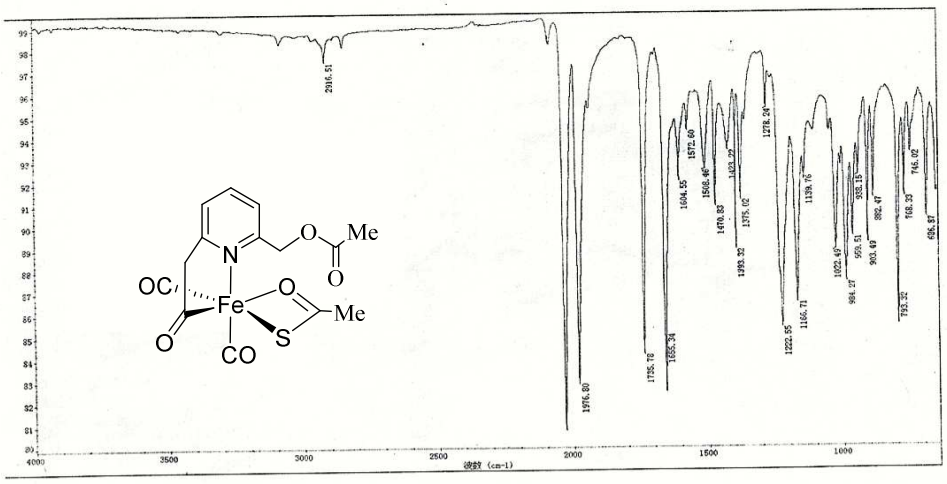

Figure S11. IR spectrum of **1**

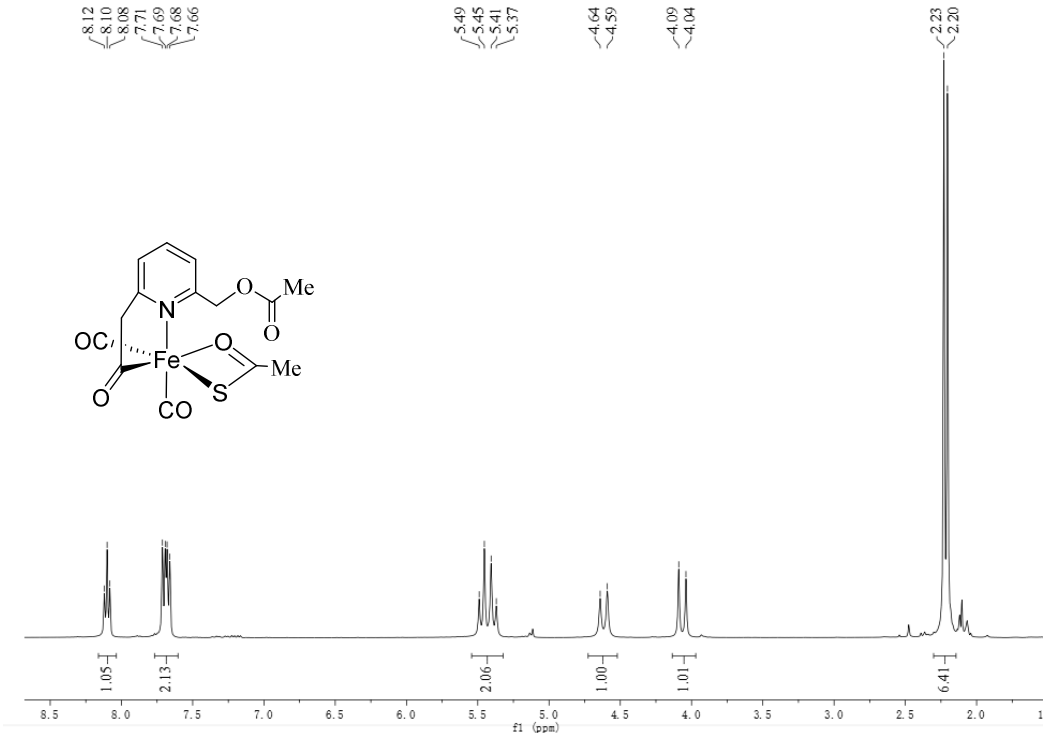

Figure S12. ^{1}H NMR spectrum of **1**

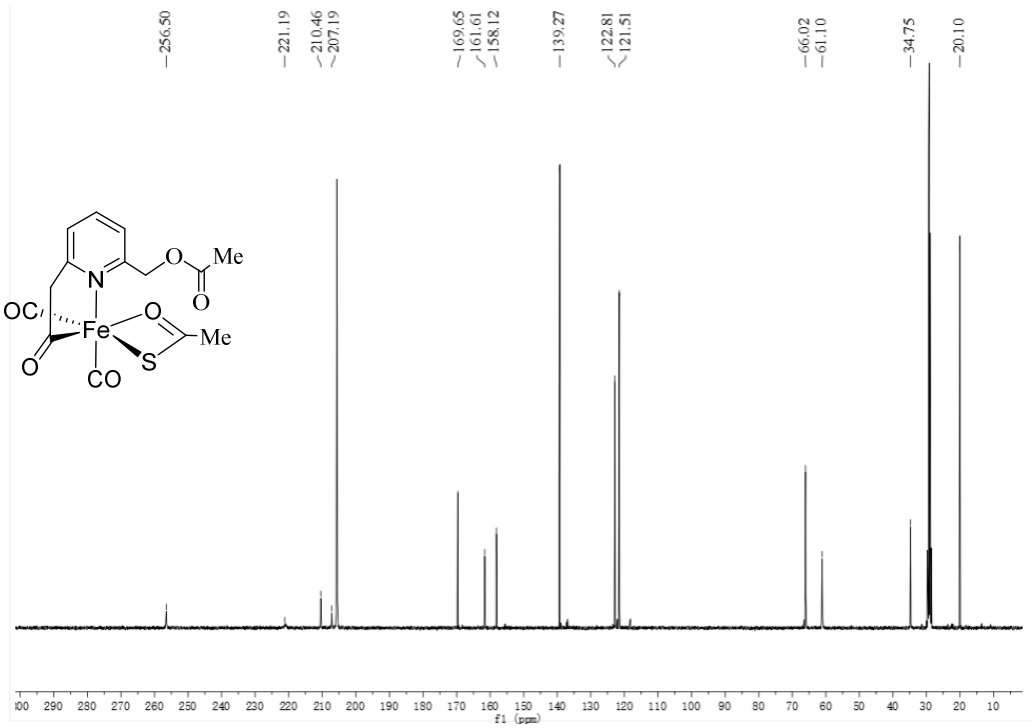

Figure S13. ^{13}C NMR spectrum of **1**

9. Figures S14–S16 IR and ^{1}H (^{13}C) NMR spectra of **2**

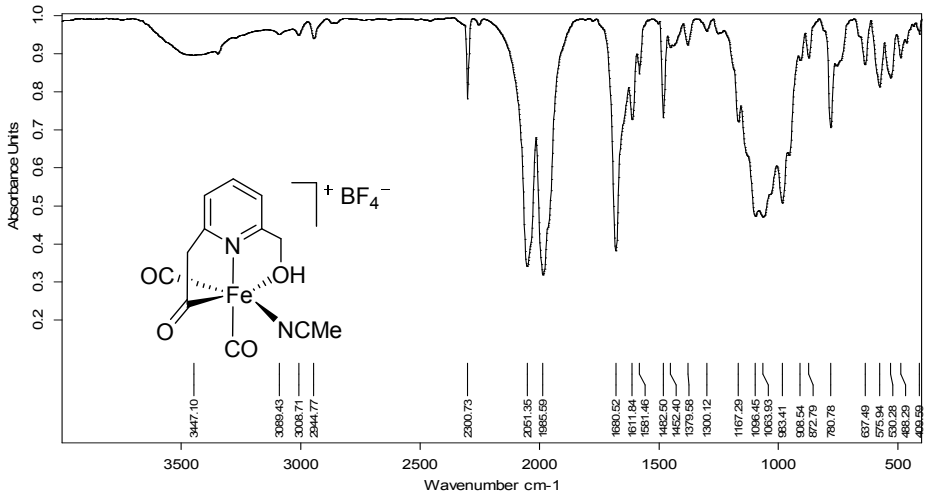

Figure S14. IR spectrum of **2**

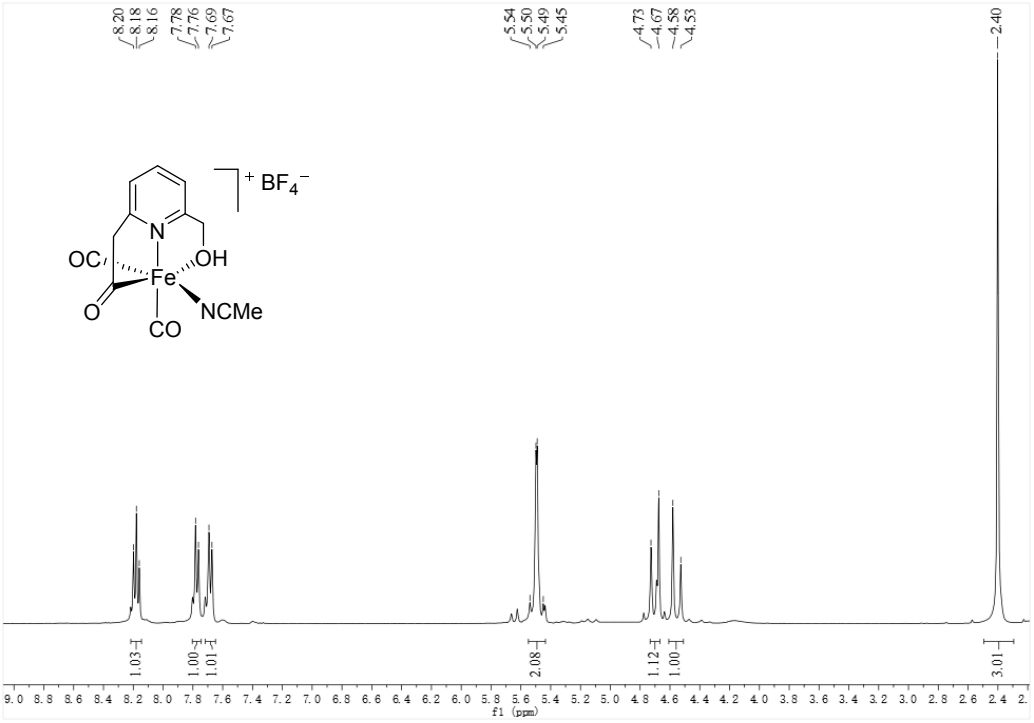

Figure S15. ^{1}H NMR spectrum of **2**

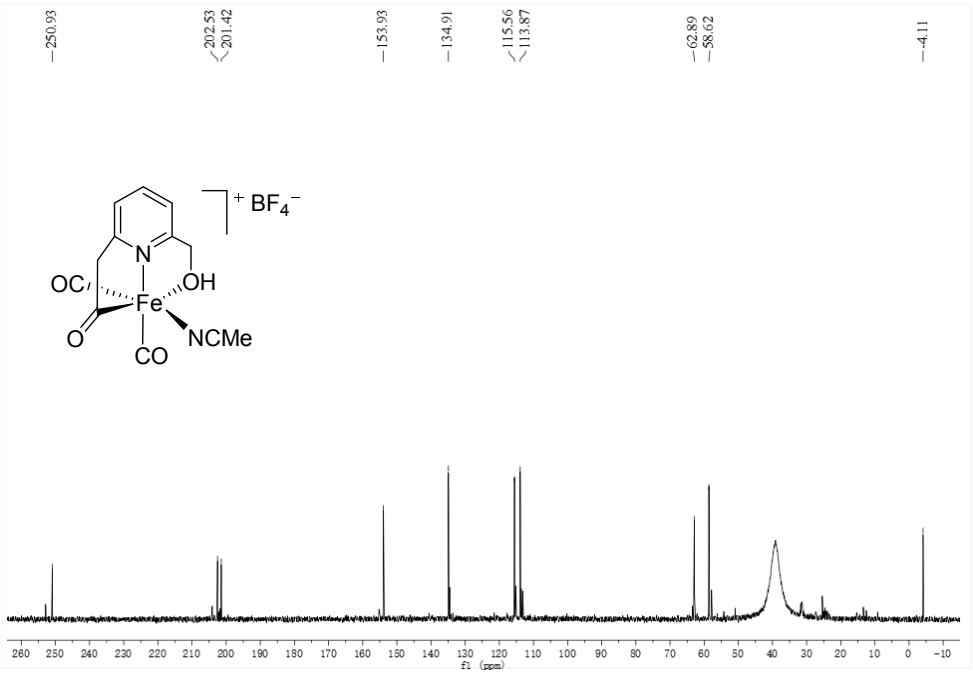

Figure S16. ^{13}C NMR spectrum of **2**

10. Figures S17–S19 IR and ^{1}H (^{13}C) NMR spectra of **3**

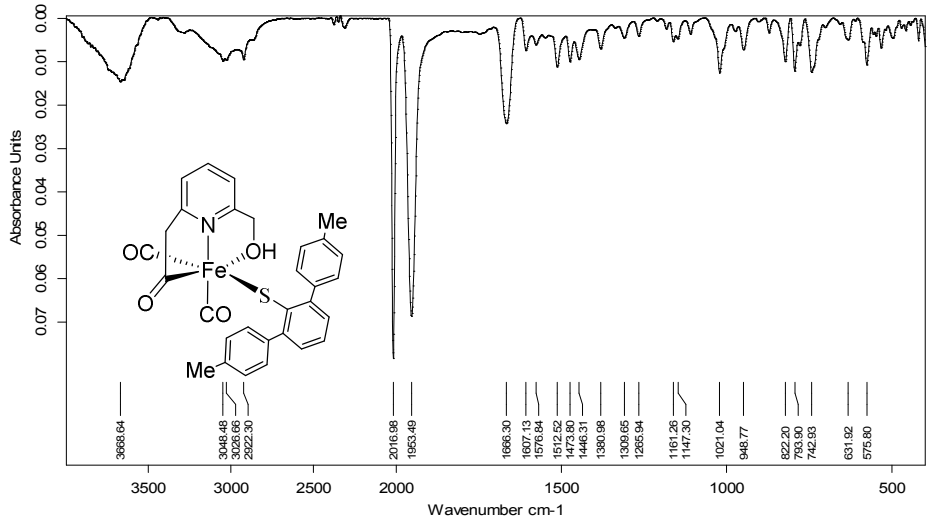

Figure S17. IR spectrum of **3**

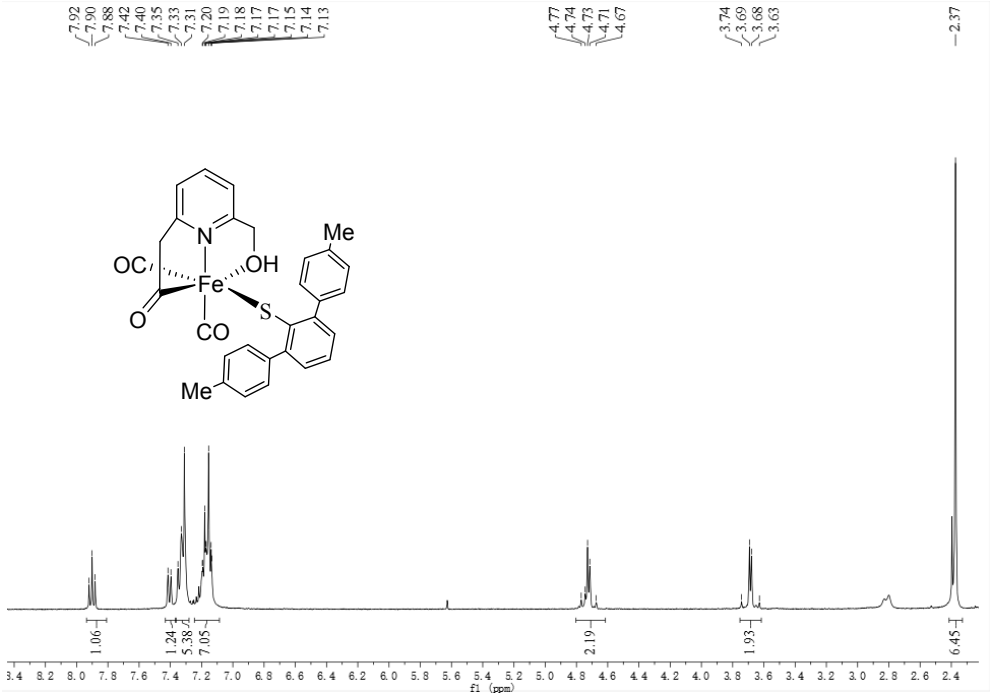

Figure S18. ^{1}H NMR spectrum of **3**

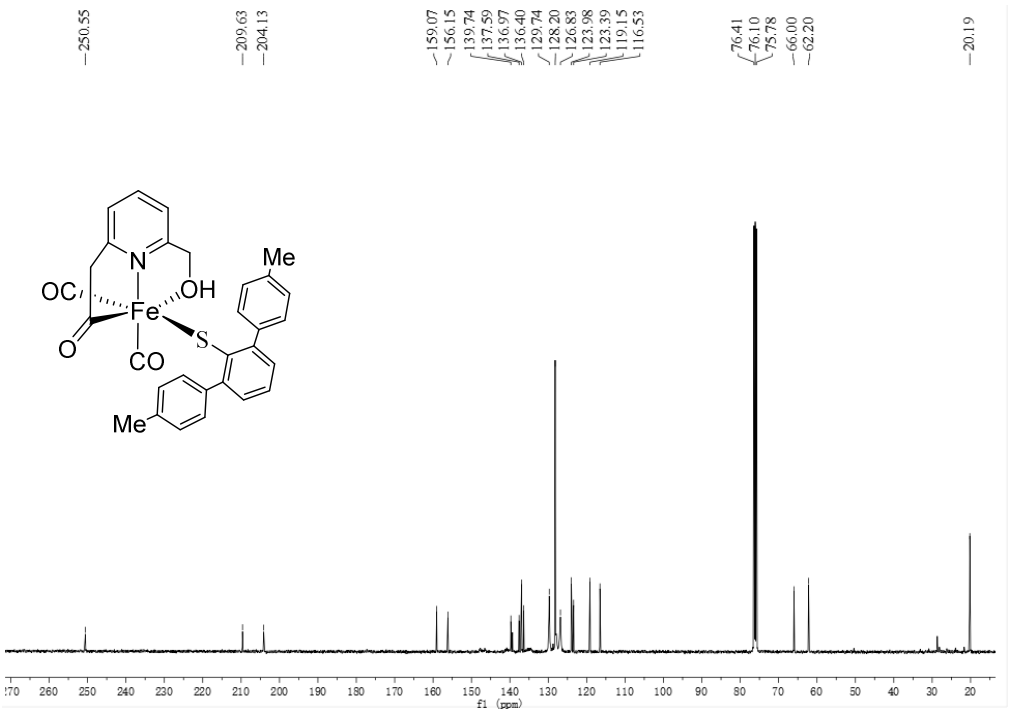

Figure S19. ^{13}C NMR spectrum of **3**

11. Figures S20–S23 IR and ^{1}H (^{13}C, ^{31}P) NMR spectra of **4**

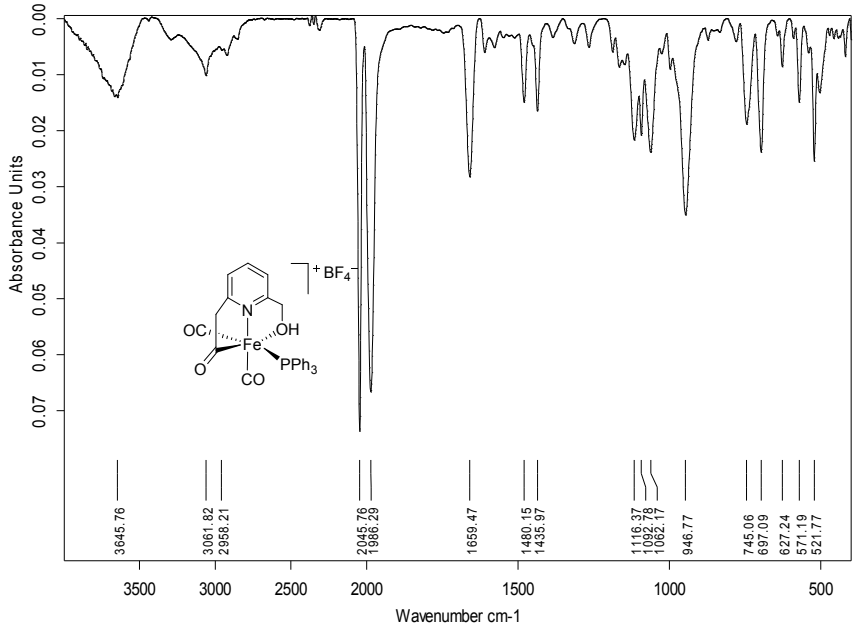

Figure S20. IR spectrum of **4**

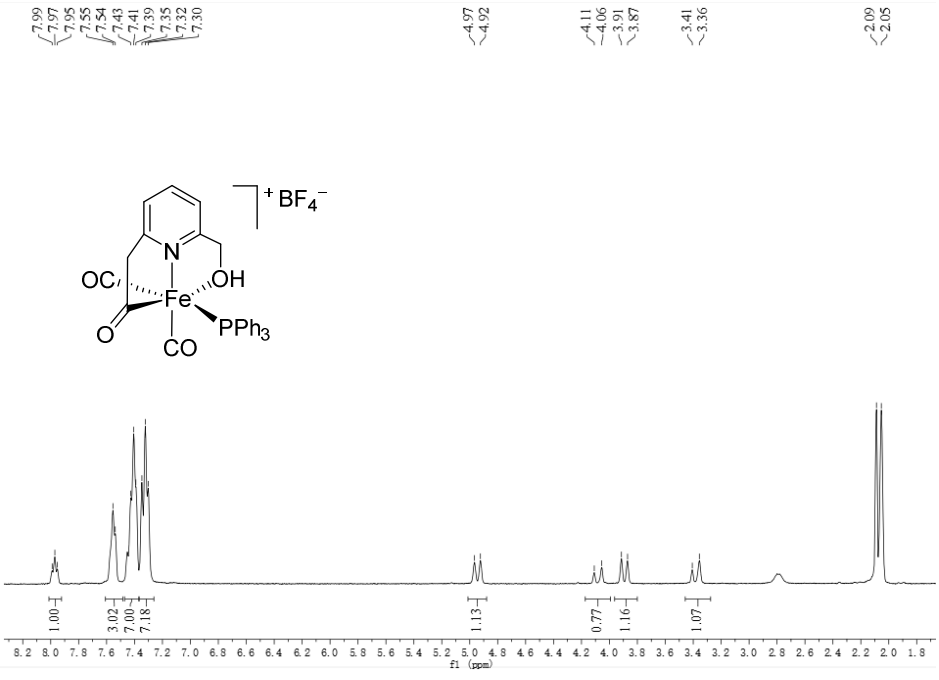

Figure S21. ^{1}H NMR spectrum of **4**

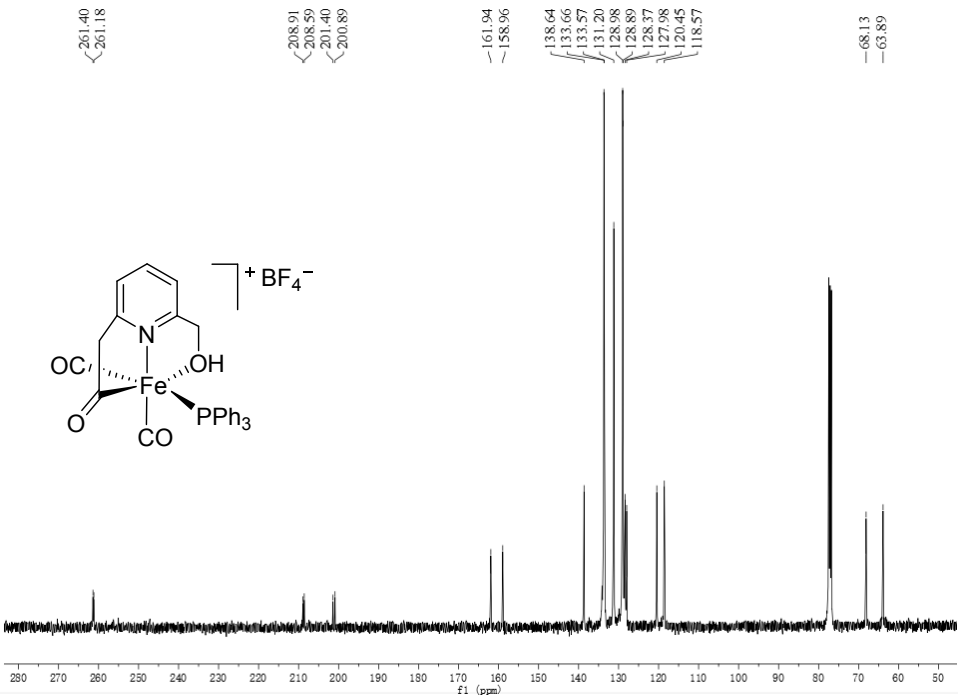

Figure S22. ^{13}C NMR spectrum of **4**

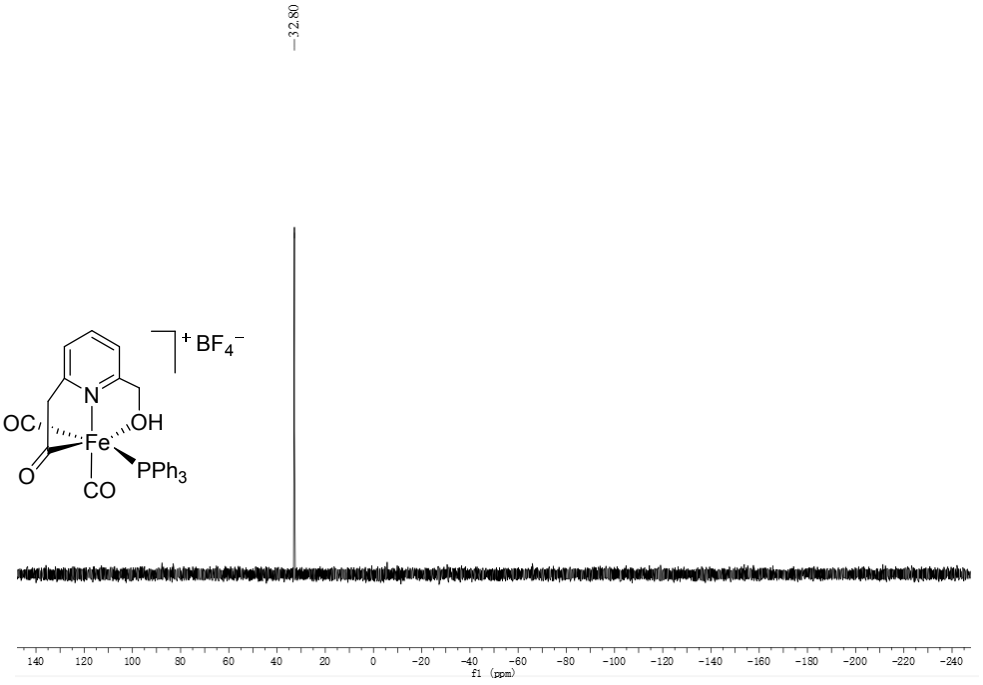

Figure S23. ^{31}P NMR spectrum of **4**

12. Figures S24–S27 IR and ^{1}H (^{13}C, ^{31}P) NMR spectra of **5**

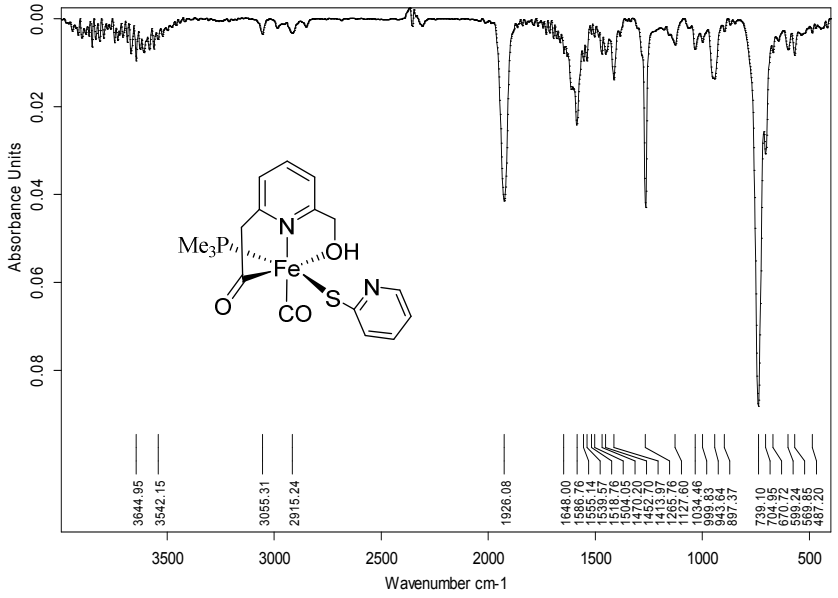

Figure S24. IR spectrum of **5**

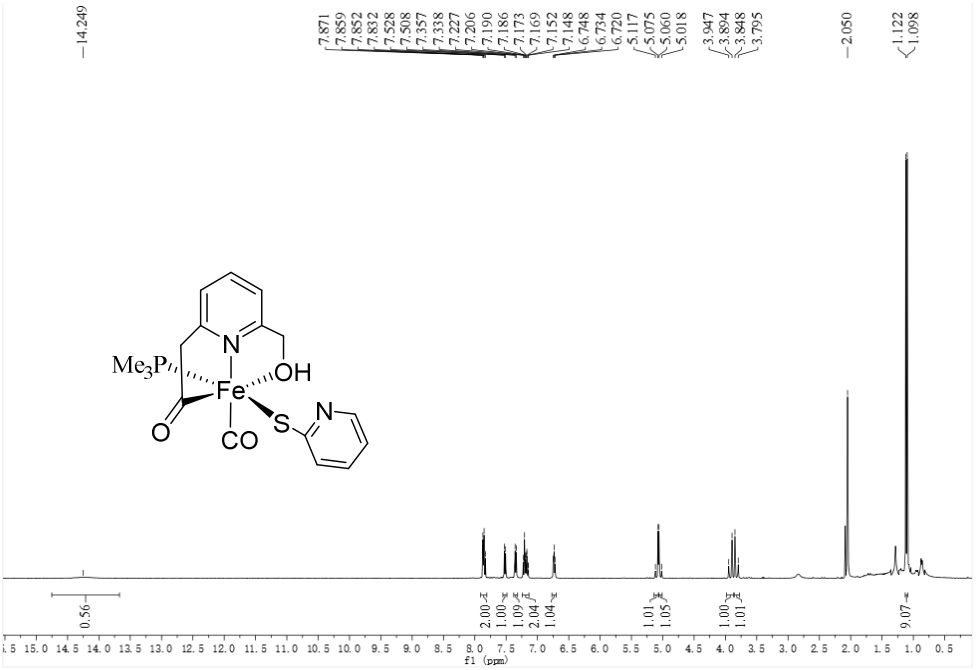

Figure S25. ^{1}H NMR spectrum of **5**

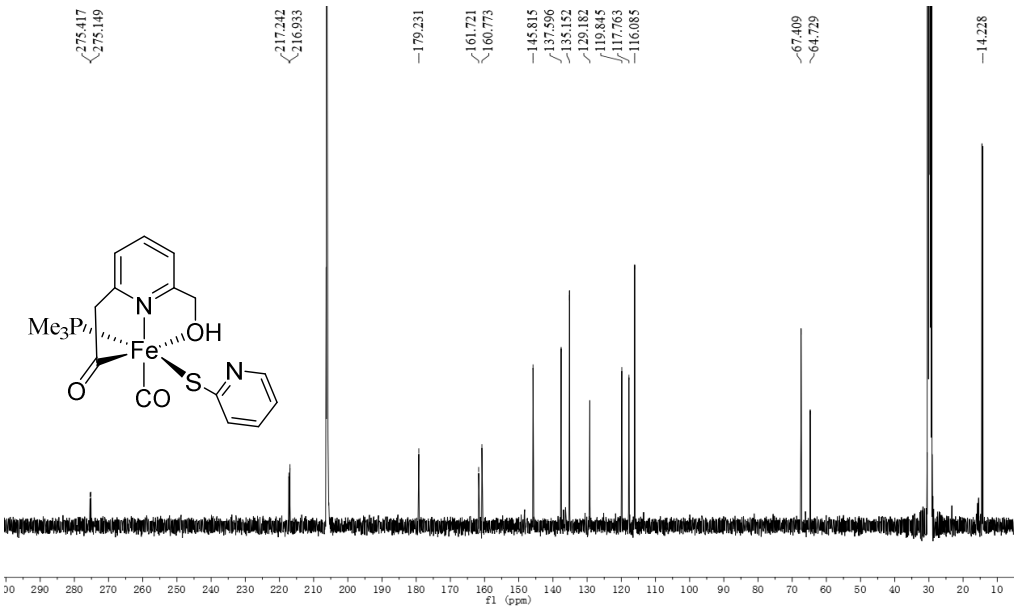

Figure S26. ^{13}C NMR spectrum of **5**

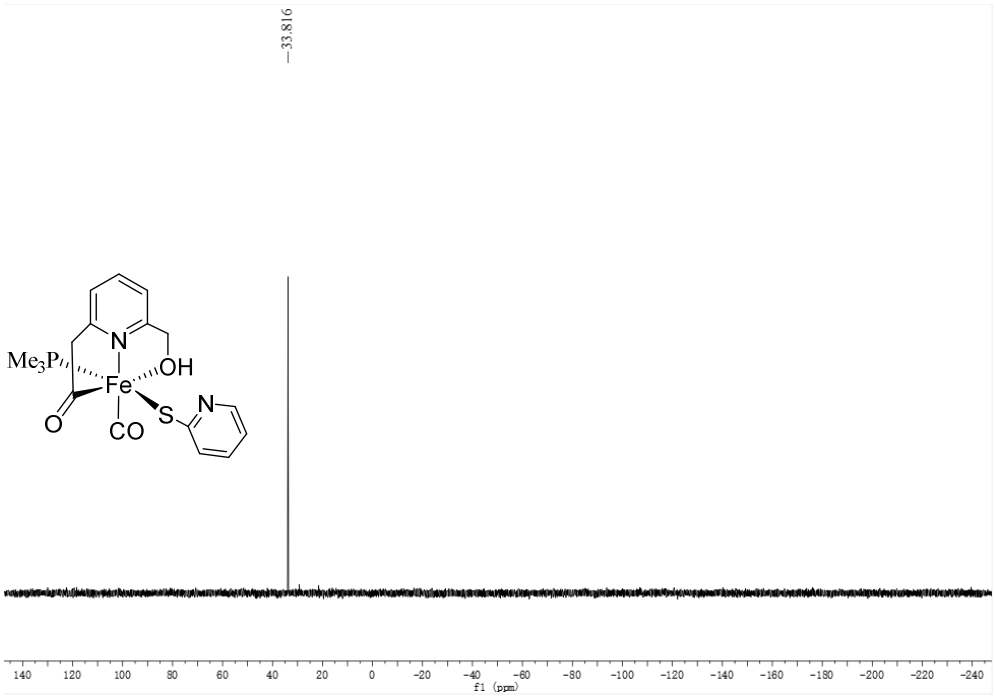

Figure S27. ^{31}P NMR spectrum of **5**

13. Figures S28–S31 IR and ^{1}H (^{13}C, ^{31}P) NMR spectra of **6**

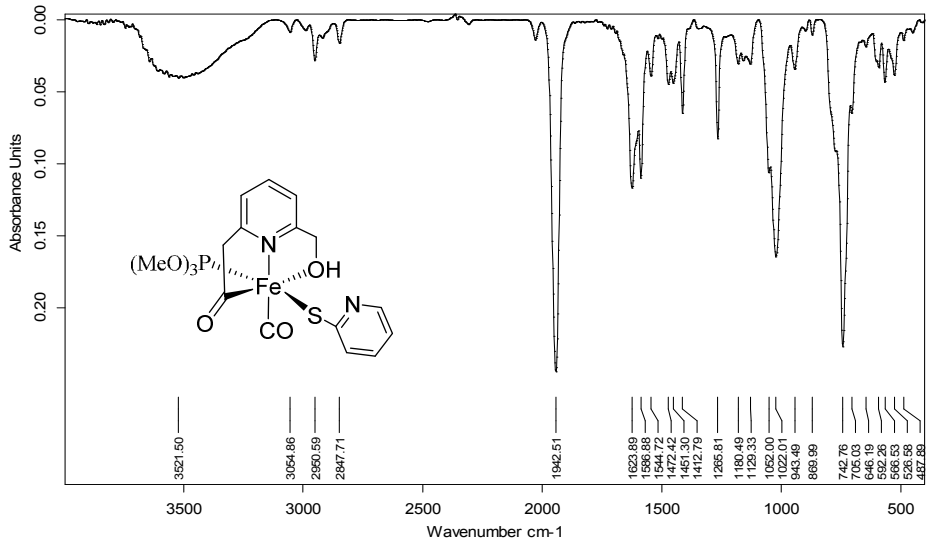

Figure S28. IR spectrum of **6**

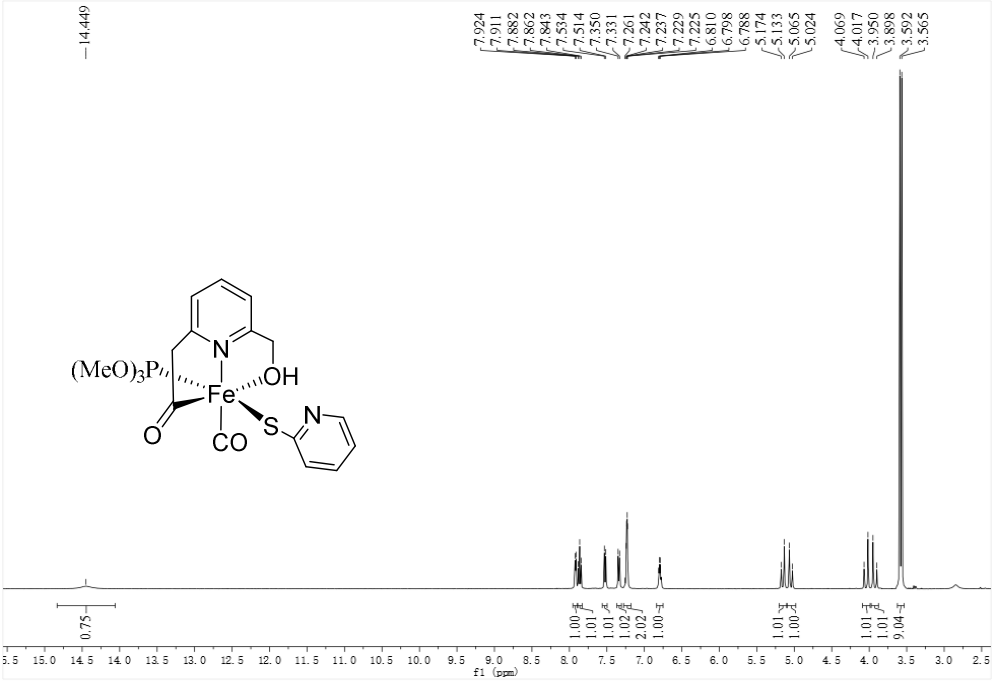

Figure S29. ^{1}H NMR spectrum of **6**

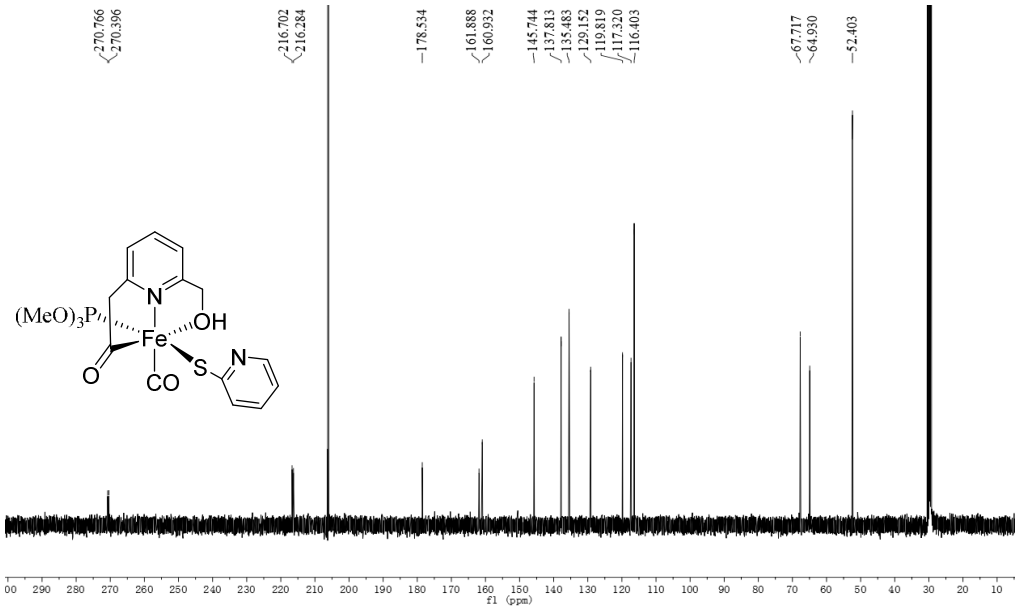

Figure S30. ^{13}C NMR spectrum of **6**

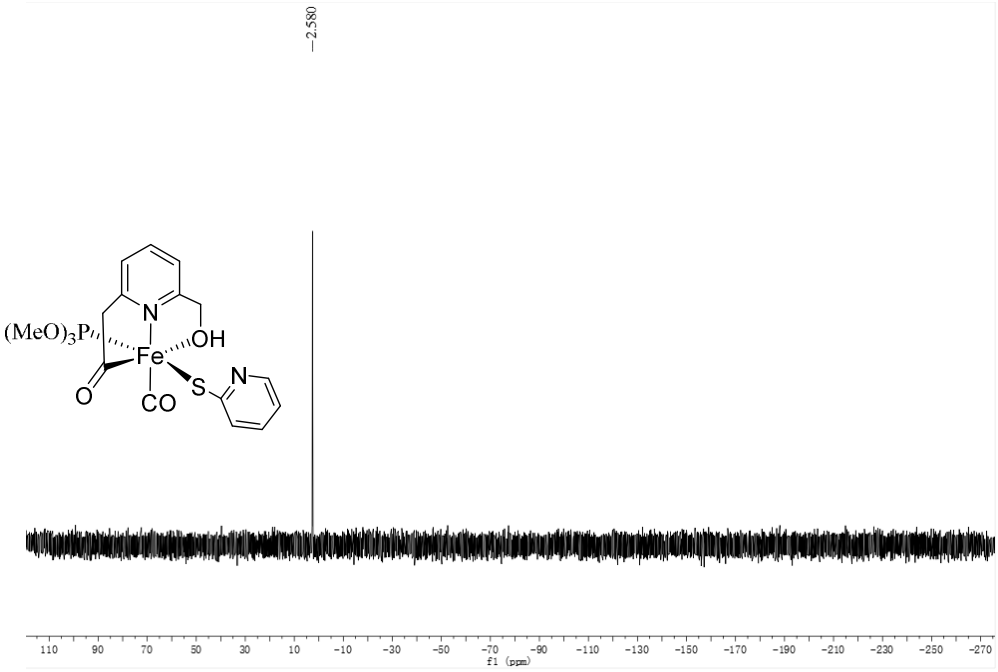

Figure S31. ^{31}P NMR spectrum of **6**

14. Figures S32–S34 IR and ^{1}H (^{13}C) NMR spectra of **7**

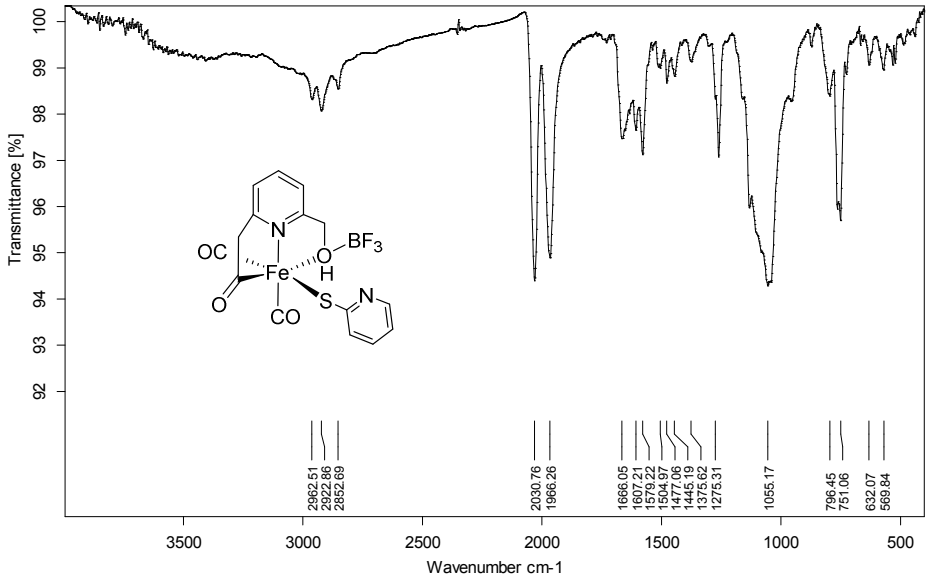

Figure S32. IR spectrum of **7**

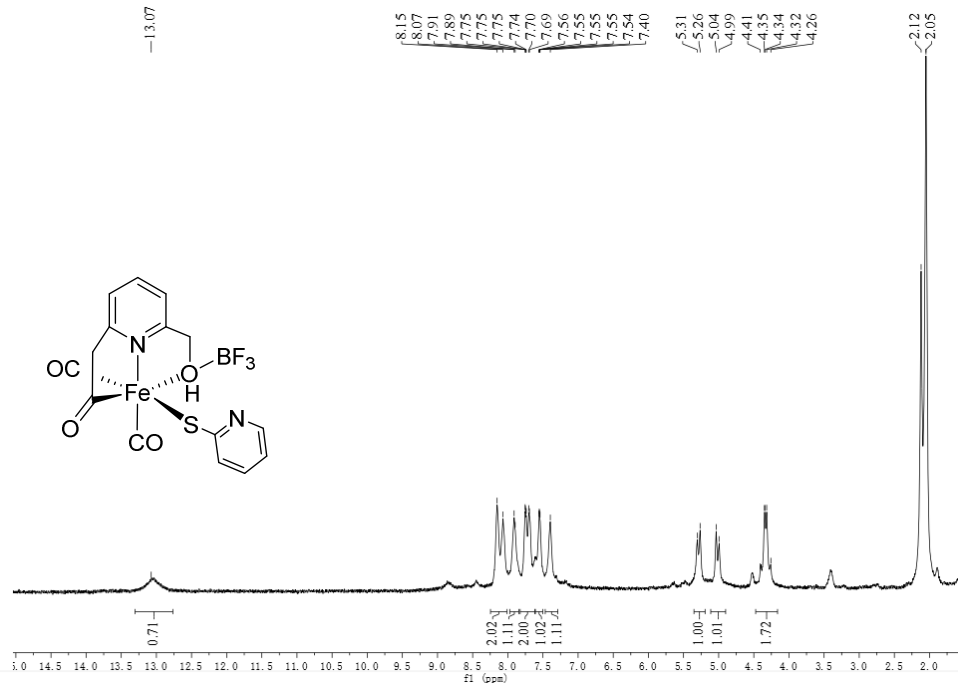

Figure S33. ^{1}H NMR spectrum of **7**

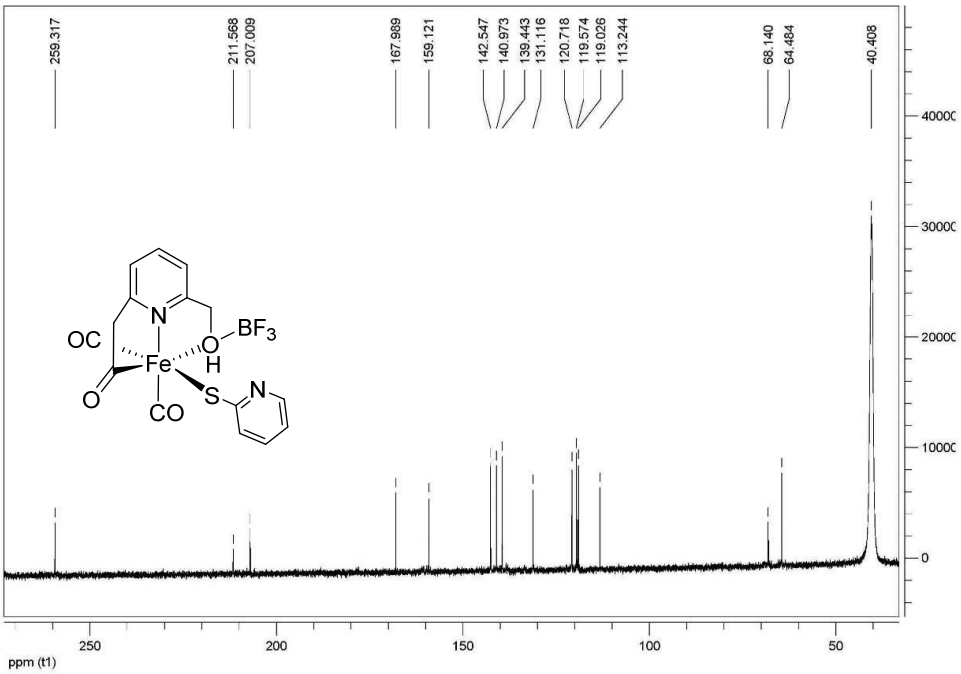

Figure S34. ^{13}C NMR spectrum of **7**

15. Figures S35–S37 IR and ^{1}H (^{13}C) NMR spectra of **8**

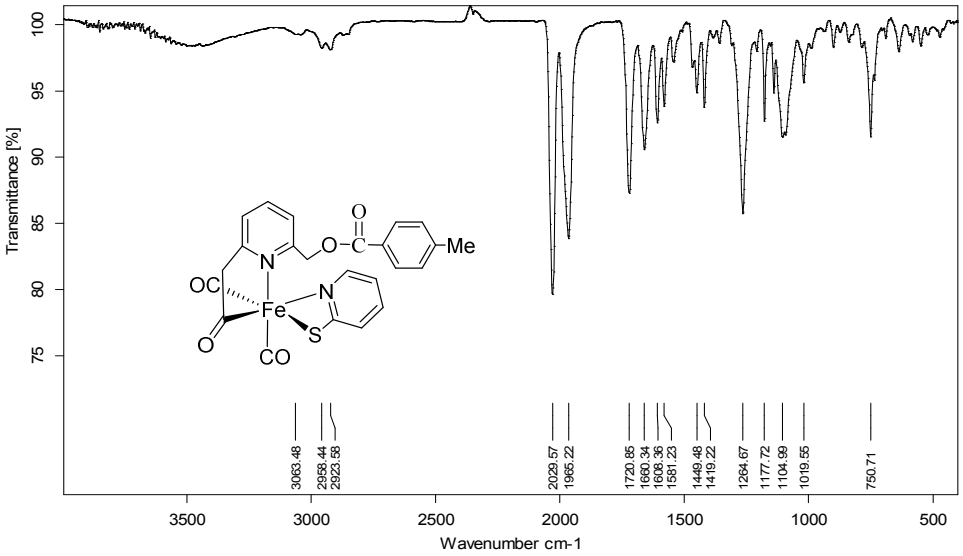

Figure S35. IR spectrum of **8**

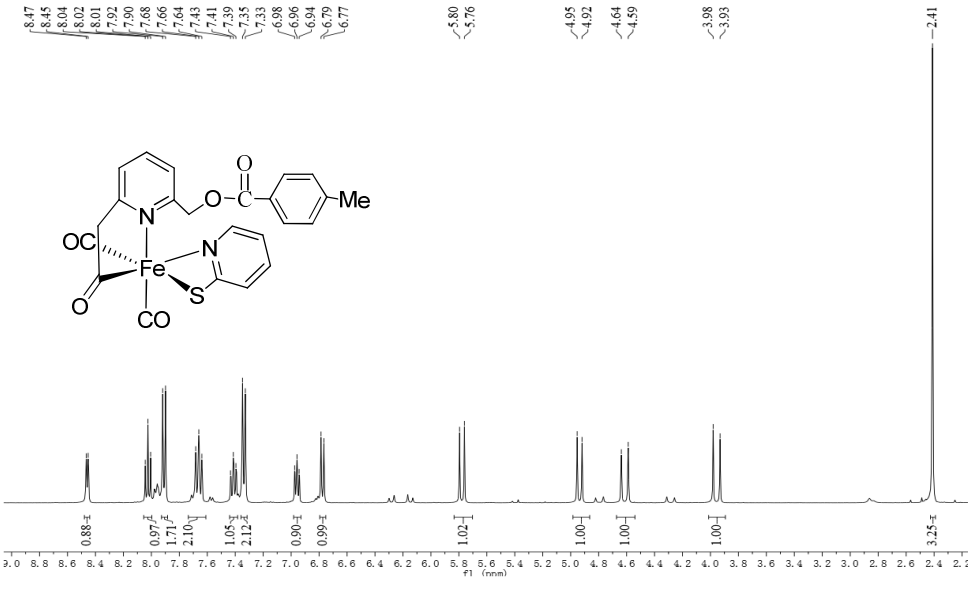

Figure S36. ^{1}H NMR spectrum of **8**

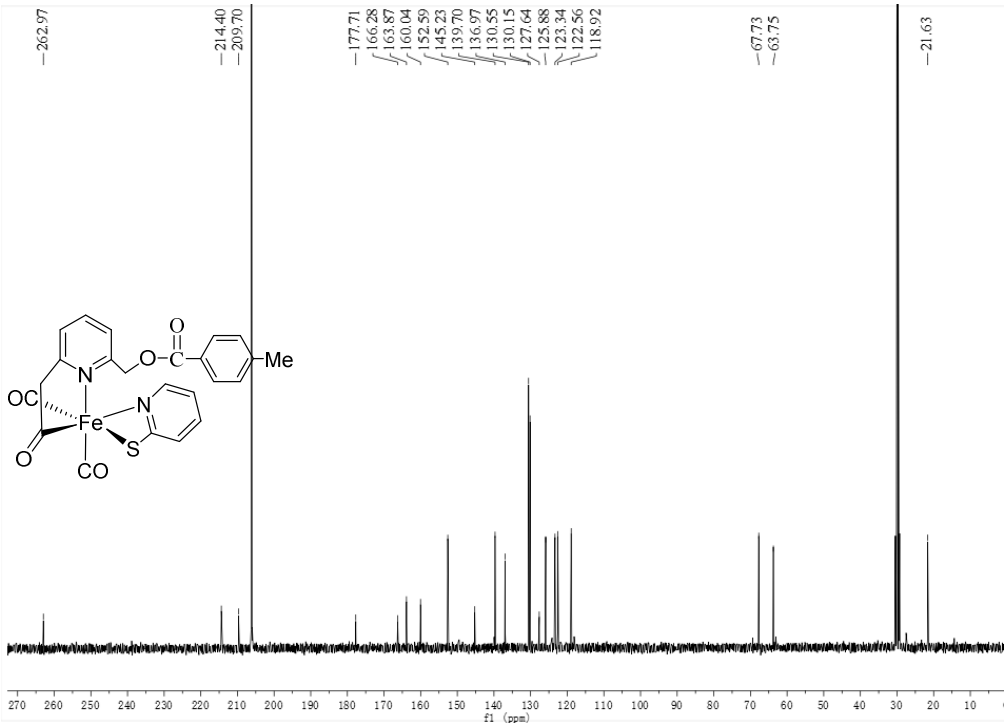

Figure S37. ^{13}C NMR spectrum of **8**

16. Figures S38–S40 IR and ^{1}H (^{13}C) NMR spectra of **9**

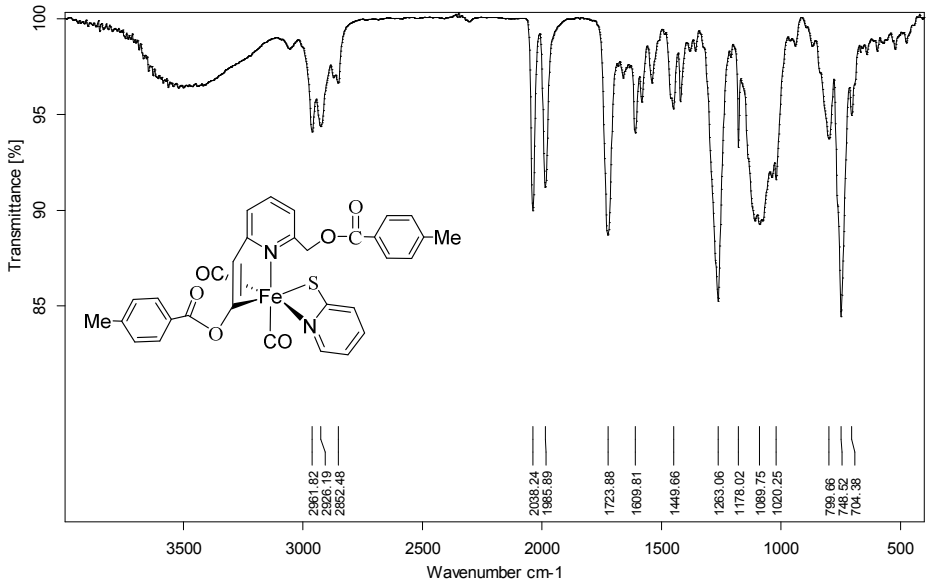

Figure S38. IR spectrum of **9**

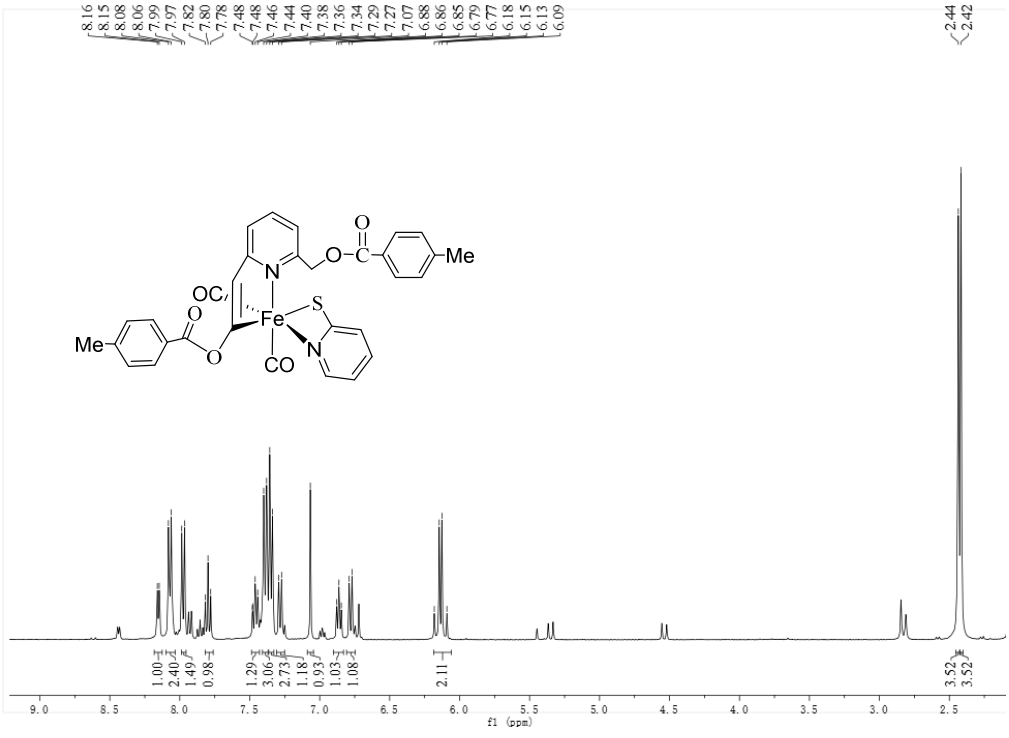

Figure S39. ^{1}H NMR spectrum of **9**

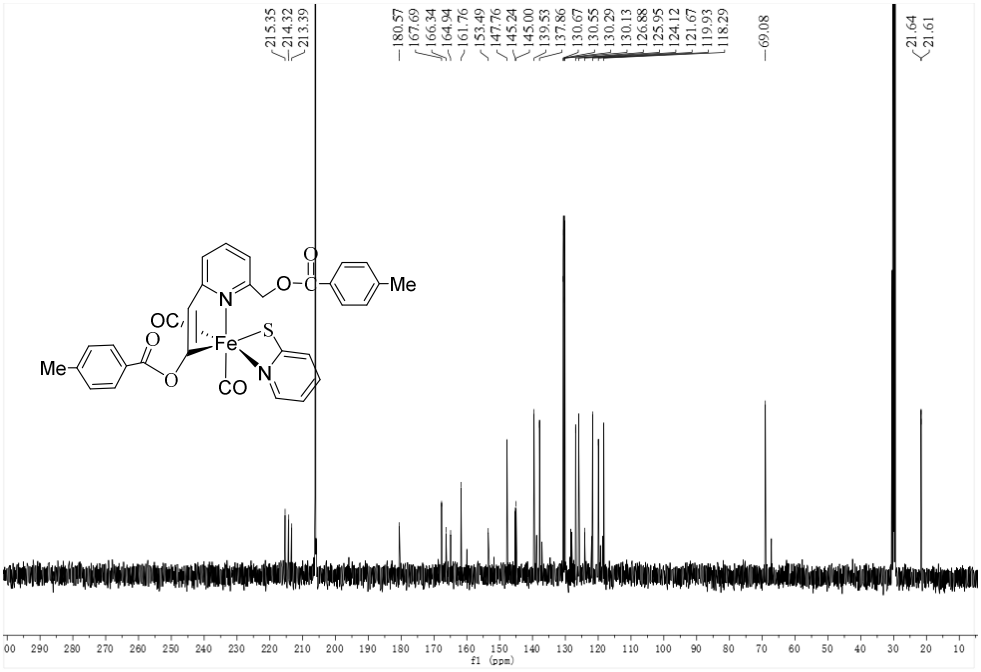

Figure S40. ^{13}C NMR spectrum of **9**

17. **References**

(1) Song, L.-C.; Gai, B.; Feng, Z.-H.; Du, Z.-Q.; Xie, Z.-J.; Sun, X.-J.; Song, H.-B. Synthesis, Structures, and Some Properties of Diiron Oxadiselenolate (ODSe) and Thiodiselenolate (TDSe) Complexes as Models for the Active Site of [FeFe]-Hydrogenases. *Organometallics* **2013**, *32*, 3673-3684.

(2) Song, L.-C.; Wang, Y.-X.; Xing, X.-K.; Ding, S.-D.; Zhang, L.-D.; Wang, X.-Y.; Zhang, H.-T. Hydrophilic Quaternary Ammonium-Group-Containing [FeFe]-Hydrogenase Models: Synthesis, Structures, and Electrocatalytic Hydrogen Production . *Chem. - Eur. J.* **2016**, *22,* 16304–16314.

(3) Kilgore, U. J.; Roberts, J. A. S.; Pool, D. H.; Appel, A. M.; Stewart, M. P.; Dubois, M. R.; Dougherty, W. G.; Kassel, W. S.; Bullock, R. M.; Dubois, D. L. $[Ni(P^{Ph}_2N^{C6H4X}_2)_2]^{2+}$ Complexes as Electrocatalysts for H_2 Production: Effect of Substituents, Acids, and Water on Catalytic Rates. *J. Am. Chem. Soc.* **2011**, *133*, 5861-5872.

(4) Wises, S. ; Kilgore, U. J. ; Ho, M.-H. ; Raugei, S. ; DuBois, D. L. ; Bullock, R. M. ; Helm, M. L. Hydrogen Production Using Nickel Electrocatalysts with Pendant Amines: Ligand Effects on Rates and Overpotentials. *ACS Catal*. **2013**, *3*, 2527-2535.

(5) Roy, S.; Nguyen, T.-A. D.; Gan, L.; Jones, A. K. Biomimetic peptide-based models of [FeFe]-hydrogenases: utilization of phosphine-containing peptides. *Dalton. Trans.* **2015**, *44*, 14865-14876.

(6) Felton, G. A. N.; Glass, R. S.; Lichtenberger, D. L.; Evans, D. H. Iron-Only Hydrogenase Mimics. Thermodynamic Aspects of the Use of Electrochemistry to Evaluate Catalytic Efficiency for Hydrogen Generation. *Inorg. Chem*. **2006**, *45*, 9181-9184.

(7) Fourmond, V.; Jacques, P.-A.; Fontecave, M.; Artero, V. H_2 Evolution and Molecular Electrocatalysts: Determination of Overpotentials and Effect of Homoconjugation. *Inorg. Chem*. **2010**, *49*, 10338-10347.

(8) Appel, A. M.; Helm, M. L. Determining the Overpotential for a Molecular Electrocatalyst. *ACS Catal*. **2014**, *4*, 630-633.